Observation Operator for Visible and Near-Infrared Satellite Reflectances

Philipp M. Kostka, *

Martin Weissmann,

Hans–Ertel–Centre for Weather Research, Data Assimilation Branch, Ludwig–Maximilians–Universität, München, Germany

Robert Buras,

Bernhard Mayer,

Meteorologisches Institut München, Ludwig–Maximilians–Universität, München, Germany

Olaf Stiller

Deutscher Wetterdienst, Offenbach, Germany

* *Corresponding author address:* Dr. Philipp Kostka, LMU Meteorologie, Theresienstraße 37, 80333 München, Germany

E-mail: philipp.kostka@lmu.de

ABSTRACT

Operational numerical weather prediction systems currently only assimilate infrared and microwave satellite observations, whereas visible and near-infrared reflectances that comprise information on atmospheric clouds are not exploited. One of the reasons for that is the absence of computationally efficient observation operators. On the road towards an operational forward operator for the future regional ensemble data assimilation system of Deutscher Wetterdienst, we have developed a version that is fast enough for investigating the assimilation of cloudy reflectances in a case study approach. The operator solves the radiative transfer equation to simulate visible and near-infrared channels of satellite instruments based on the one-dimensional (1D) discrete ordinate method. As input, model output of the operational limited area forecasting model of Deutscher Wetterdienst, is used. Assumptions concerning subgrid-scale processes, calculation of in-cloud values of liquid water content, ice water content and cloud microphysics are summarized and the accuracy of the 1D simulation is estimated through comparison with three-dimensional (3D) Monte Carlo solver results. In this context, also the effects of a parallax correction and horizontal smoothing are quantified. The relative difference between the 1D simulation in ”independent column approximation” and the 3D calculation is typically less than 9 % between $06 - 15$ UTC. The parallax corrected version reduces the deviation to less than 6 % for reflectance observations with a central wavelength of 810 nm. Horizontal averaging can further reduce the error of the 1D simulation. In all cases, the systematic difference is less than 1 % for the model domain.

1. Introduction

Extending the use of satellite radiances for numerical weather prediction (NWP) is a strong priority at many forecast centers. While the assimilation of satellite radiances has led to some of the greatest increases in forecast skill that have been achieved during the last decade, the current use of satellite radiances is still very restrictive with only a small fraction of the available observations being included in the data assimilation (DA) process. Particularly, a better exploitation of cloud or precipitation affected satellite measurements could bear great potential for further improvements of weather forecasting (Bauer et al. 2011a). These data specifically provide information from overcast regions which are typically sensitive regions with great importance for NWP (McNally 2002). In particular, information linked to cloud variables and precipitation could help to improve the forecast of convective precipitation which is one of the key targets for regional high resolution limited area models.

The assimilation of radiances that are affected by clouds or precipitation is, however, much more difficult than in clear air (Errico et al. 2007). Crucial reasons for this are the complexity and non-linearity of the relevant forward operators that increase substantially in the presence of water in the condensed or frozen phase, see e.g. Bennartz and Greenwald (2011). Such forward operators (also called observation operators) which compute the model equivalent for the respective observation types are vital parts of modern DA systems. For variational DA systems, also their linearized and adjoint versions are required, while for ensemble DA systems the forward operator itself is sufficient.

For satellite radiances, the forward operator includes a radiative transfer (RT) model which computes the radiances that would be measured by the satellite instrument for a given atmospheric state. In the presence of clouds these RT computations can become very demanding (Liou 1992), especially in the solar spectral range, while a crucial requirement for developing a DA system that can deal with cloudy radiances is a sufficiently fast and reliable RT model for the respective wavelengths.

So far, most of the radiance assimilation efforts (including those concerning cloud affected measurements) were made for global models (i.e. synoptic scale) and focused on radiation in the microwave (MW) or infrared (IR) spectral bands (Bauer et al. 2011b). In some respect, the situation is easiest for the MW spectrum, where clouds are usually transparent and only very thick water clouds and rain perturb the signal. As a consequence, the corresponding RT operator is much more linear than for IR radiances and an all sky approach has been successfully adopted at the European Centre for Medium-Range Weather Forecasts (Bauer et al. 2010).

For IR radiances, RT computations are substantially more non-linear and very sensitive to the input cloud variables. For this reason, assimilation methods have been developed that intend to "subtract" the influence of clouds on the RT computations in order to assimilate the same fields as for clear air assimilation despite the presence of clouds (McNally 2009; Pavelin et al. 2008; Pangaud et al. 2009) rather than exploiting the cloud information contained in the cloudy radiances. The temperature and humidity fields constrain the occurrence of clouds to a certain extent, but the full observed information on clouds is not directly assimilated.

A central task for limited area models is to produce a more accurate short term forecast of clouds and precipitation. For the initialization of such models the explicit exploitation of cloud information therefore has higher priority than for global models. Recent efforts on the assimilation of information from cloud and rain contaminated remote sensing data are presented in Renshaw and Francis (2011), Storto and Tveter (2009), Chevallier et al. (2004), Stengel et al. (2012) and Stengel et al. (2010).

While most of the radiance assimilation so far has focused on the IR and MW radiances, in particular clouds at lower levels have a clearer signal in the solar spectral range. In addition, the solar channels contain quantitative information about the liquid water content in clouds while the IR signal quickly saturates in clouds and thus only provides information about the presence of clouds and the temperature at cloud tops. If the aim is to exploit cloud information, it seems natural to draw the attention to these wavelengths even though the corresponding RT computations are comparably complex. In this paper, we present a forward operator for radiances in the visible (VIS) and near-infrared (NIR) spectral range for the pre-operational regional Km-scale Ensemble Data Assimilation (KENDA) system of Deutscher Wetterdienst (DWD) that is based on a Local Ensemble Transform Kalman Filter (LETKF, Hunt et al. (2007)).

In the past, many decisions with respect to wavelength selection and assimilation strategy were made with regard to variational DA systems that are extremely demanding concerning the linearizability of the forward operator as strong non-linearities can endanger the convergence of the minimization of the cost function. Lately, many operational centers started to develop DA systems based on Ensemble Kalman Filter (EnKF) methods for their limited area models. While these also make assumptions about the linearity of the assimilation problem, they are expected to be more robust with respect to the occurrence of non-linear effects (Kalnay et al. 2008). Since the assimilation of cloud information is a great priority for these models, we believe that the assimilation of VIS and NIR radiances yields a great potential.

The paper is structured as follows. Section 2 introduces the configuration of the operational limited area COSMO (COnsortium for Small-scale MOdeling) model used at DWD and its relevant output for the RT calculations. Furthermore, the concept of RT and the particular solvers applied in this article are described. In section 3, important parameterizations used in the forward operator are summarized. These include the total liquid and ice water content calculated from both grid-scale model variables and assumptions about the subgrid-scale cloud water mass fractions (liquid and frozen). In addition, the parameterizations of effective scattering radii of water droplets and ice crystals in clouds are given. Section 4 describes the pre-processing parallax correction that is applied to simulate 1D RT in columns tilted towards the satellite to account for the slant viewing angle. The accuracy assessment based on the comparison of 1D and 3D results is presented in section 5 and a summary is given in section 6.

2. Models

This section provides a description of the limited area COSMO-DE configuration of the operational model used at DWD, the processing of its output to synthetic satellite images using forward operators and the main properties of the employed 1D and 3D RT solvers used in this study.

a. Meteorological Model and Data

The forecast fields used to simulate synthetic satellite images are produced by the COSMO community model. The COSMO model has been used for operational numerical weather prediction at DWD since 1999. The convection-permitting model configuration COSMO-DE has been operational since April 2007. The model domain has a horizontal grid-spacing of 2.8 km and consists of 421×461 grid points. The area covers Germany as well as Switzerland, Austria and parts of the other neighboring countries of Germany. In the vertical, it consists of 50 model layers. The model explicitly resolves deep convection, while shallow convection is parameterized (Baldauf et al. 2011).

The VIS and NIR operator uses the model output of temperature, pressure, mass fractions of humidity, cloud liquid water, cloud ice and snow, as well as cloud-cover in each layer and the base and top heights of shallow convective clouds. In addition, the temporally constant parameters orography, geometrical height of model layer boundaries, latitude and longitude are input for the operator. As a case study, 22 June 2011 has been chosen and output fields from 3h-forecasts at 06, 09, 12, 15 and 18 UTC have been used for the simulations. This is a particularly interesting day from the meteorological point of view since on 22 June 2011 a well-developed cold front at the leading edge of an upper-level trough passed Germany. A strong jet streak at 500 hPa overlapped with low-level instability providing favorable conditions for deep convection. Heavy rain, hail, strong winds and a tornado were observed in central Germany.

b. *Radiative Transfer Models*

As a tool to simulate RT for solar radiation, the software package libRadtran by Mayer and Kylling (2005) is applied. It contains the *uvspec* model, a command line based executable to solve RT using ASCII input files. The input files are used to concisely define an atmospheric scene in terms of, e.g., water and ice clouds represented by their liquid water content (LWC), ice water content (IWC), surface albedo, trace gases, aerosol, etc. In combination with information about microphysical cloud properties such as the effective radii of scattering particles, optical properties are calculated. The parameterizations used to calculate LWC, IWC and the corresponding effective radii are described in section 3. Subsequently, the optical properties given in terms of the extinction coefficient, the single scattering albedo and the scattering phase function are passed on to the RT solver which calculates radiative quantities such as radiances or reflectances. Finally, a post-processing of the output takes into account the extraterrestrial solar spectrum, the Earth-Sun distance and so forth.

libRadtran includes several RT solvers of varying complexity and degree of approximation. In the context of this study, two solvers are applied. The first one is the 1D solver based on the discrete ordinate method (DISORT) by Stamnes et al. (1988), modified and translated into C-code by Buras et al. (2011) that is used in our proposed forward operator. The second one is the Monte Carlo code for the physically correct tracing of photons in cloudy atmospheres (MYSTIC) 3D solver (Emde and Mayer 2007; Mayer 2009; Buras and Mayer 2011) that is used as "model truth".

Each solver provides a numerical solution to the radiative transfer equation (Chandrasekhar 1960),

$$\frac{\mathrm{d}L}{\beta\,\mathrm{d}s} = -L + \frac{\omega}{4\,\pi}\int P(\mathbf{\Omega},\mathbf{\Omega}')\,L(\mathbf{\Omega}')\,\mathrm{d}\mathbf{\Omega}' + (1-\omega)\,B(T)\,, \tag{1}$$

where L denotes the radiance for a certain location and direction, β is the volume extinction coefficient, ω the single scattering albedo, $B(T)$ the Planck function and $P(\mathbf{\Omega},\mathbf{\Omega}')$ the scattering phase function determining the probability of scattering from a beam direction $\mathbf{\Omega}'$

to $\mathbf{\Omega}$. For the case at hand, where the focus lies on RT in the solar channels, the emission given by the last term involving $B(T)$ is negligible for VIS and comparably small for NIR.

The 1D solver DISORT solves Eq. (1) in a horizontally homogeneous plane-parallel atmosphere[1] by discretizing into a finite amount of angular streams s on which the scattering integral is evaluated in terms of Gaussian quadrature. For this purpose, the scattering phase function is expanded into a finite series of Legendre polynomials.[2] The RT equation is solved in each of the n_z atmospheric layers with constant optical properties. Thus, a total number of $2\,s\,n_z$ equations has to be evaluated, where continuity requirements for the radiance field need to be satisfied at the level interfaces. In the presented examples, n_z is set to 50 and the number of angular streams s is set to 16.

The Monte Carlo solver MYSTIC is a probabilistic approach to the solution of Eq. (1). It traces model photons on their way through the atmosphere. Scattering and absorption in the atmosphere and reflection and absorption at the ground are accounted for. At each interaction point, the properties (e.g. type of extinction process, scattering angles in the case of scattering, etc.) are drawn randomly using the respective cumulative probability density and the Mersenne-Twister MT 19937 random number generator (Matsumoto and Nishimura 1998). The length of a path in between interaction grid boxes can be calculated by integrating the extinction coefficient along the path until the optical depth drawn randomly from the inverse Lambert-Beer probability density is reached. These steps are repeated for a large number of model photons.

For our application, we are interested in satellite radiances (or equivalently reflectances), which are difficult to obtain from standard Monte Carlo simulations, because the photons rarely hit the detector, let alone coming from the direction of viewing. Therefore so-called variance reduction techniques are used which increase the efficiency by several orders of magnitude. We use the backward Monte Carlo approach where photons are generated in the

[1] Meaning a horizontally infinitely extended model atmosphere with parallel layers in which optical properties only vary vertically.

[2] A detailed description is given in Zdunkowski et al. (2007) to which the interested reader is referred.

final detector direction on random pixel positions at top of the atmosphere and travel backwards. At each interaction with the atmosphere or surface, a local estimate is performed, i.e. the probability that the photon scatters/reflects towards the sun and is not extinct on its subsequent way through the atmosphere is calculated. The sum of all local estimates yields the correct result for the radiance measured by the satellite, as can be proven with the von Neumann rule (Marchuk et al. 1980). For a detailed description of the local estimate technique, see Mayer (2009). Due to convergence problems arising when using the local estimate technique in the presence of clouds, we also use the set of variance reduction techniques VROOM described in Buras and Mayer (2011).

The main uncertainty of MYSTIC is the statistical photon noise (roughly proportional to $1/\sqrt{N}$) which is small provided that the number of photons N is large enough. For the purpose of this study, the 3D RT simulations will be considered as "model truth" against which the results of the 1D operator are verified. The big disadvantage of the Monte Carlo method is certainly the excessively large amount of computer time required to obtain a result with a small statistical error ($t \sim N \sim \sigma^{-2}$). Therefore, it remains a good research tool for producing very realistic simulations, however its capability for operational applications, e.g., observation operators for cloudy satellite radiances, is very limited with current computer systems.

For the parameterization of molecular absorption, the LOWTRAN band model by Pierluissi and Peng (1985) has been applied as adopted from the SBDART code by Richiazzi et al. (1998). Thus, a three-term exponential fit[3] is used for the transmission which implies that one simulation corresponds to three solutions of the RT equation for one spectral increment. Standard pre-calculated Mie lookup-tables are used for scattering by water droplets. The scattering tables are based on the algorithm described in Wiscombe (1979, edited and revised 1996). For the scattering of radiation by ice crystals, the parameterizations by Baum

[3]According to Wiscombe and Evans (1977) it is necessary to express the transmission as a sum of several exponential functions.

et al. (2005a), Baum et al. (2005b) and Baum et al. (2007) are used.

Within this article, the calculated radiance is converted to reflectance, defined by

$$R = \frac{\pi \cdot L}{E_0 \, \cos\theta_0} \,, \tag{2}$$

where E_0 denotes the extraterrestrial flux and θ_0 the solar zenith angle (SZA).

3. Parameterizations

Due to unresolved processes in the model, assumptions about subgrid-scale contributions to liquid and frozen cloud water have to be implemented as parameterizations in the forward operator besides approximations about the sizes of scattering particles.

a. *Liquid and Ice Water Content*

The input parameters to the forward operator are the grid-scale fields of pressure P, temperature T and the mass fractions of humidity Q_V, liquid cloud water Q_C, cloud ice Q_I and snow Q_S. Model fields of cloud-cover CLC as well as the base height $H_\mathrm{SC}^\mathrm{bas}$ and top height $H_\mathrm{SC}^\mathrm{top}$ of shallow convective clouds are also input for the forward operator. The cloud related input variables (Q_C, Q_I and Q_S) are all grid-scale quantities. To include the impact of subgrid processes in the calculations of radiation, the COSMO model uses a subgrid parametrization which derives the respective cloud variables $Q_\mathrm{rad}^\mathrm{water}$ and $Q_\mathrm{rad}^\mathrm{ice}$ used in the model's radiation scheme. To derive the input quantities for the RT solver, the VIS and NIR forward operator largely follows this subgrid scheme. The only difference is that the forward operator replaces the input variable Q_I by a mixed variable $\tilde{Q}_\mathrm{I} = Q_\mathrm{I} + 0.1\, Q_\mathrm{S}$. This slightly revises the separation between ice and snow carried out by the COSMO model whose radiative interaction has been tuned with respect to thermal radiation only.

In the subgrid scheme of the COSMO model, the grid-scale input variables Q_C and Q_I only serve to specify lower bounds for the subgrid variables $Q_\mathrm{sgs}^\mathrm{water}$ and $Q_\mathrm{sgs}^\mathrm{ice}$ of in-cloud water mass fractions (liquid and frozen) from which $Q_{\mathrm{rad}}^{\mathrm{water}}$ and $Q_{\mathrm{rad}}^{\mathrm{ice}}$ are derived. Apart from these lower bounds, $Q_{\mathrm{sgs}}^{\mathrm{water}}$ and $Q_{\mathrm{sgs}}^{\mathrm{ice}}$ are determined

i) by the assumption that the subgrid in-cloud water Q_{sgs} is half a percent of the saturation value, i.e., $Q_{\mathrm{sgs}} = 0.005\, Q_{\mathrm{sat}}$, and

ii) by the partitioning of Q_{sgs} which is done through a simple temperature dependent coefficient f_{ice}, i.e., $Q_{\mathrm{sgs}}^{\mathrm{water}} = Q_{\mathrm{sgs}}\,(1 - f_{\mathrm{ice}})$ and $Q_{\mathrm{sgs}}^{\mathrm{ice}} = Q_{\mathrm{sgs}}\, f_{\mathrm{ice}}$.

As seen from Eq. (A6) the coefficient f_{ice} decreases linearly from the value of one for temperatures below -25°C to zero at -5°C (and above). This coefficient is also used in the definition of the effective saturation value Q_{sat} which is a linear combination of the saturation values over liquid water $Q_{\mathrm{sat}}^{\mathrm{water}}$ and ice $Q_{\mathrm{sat}}^{\mathrm{ice}}$ respectively, see appendix Eqs. (A5) and (A3) for definitions.

Apart from Q_{sgs}, the subgrid scheme also considers cloud water contributions from shallow convective clouds which are treated separately as this process is parametrized in the COSMO model. Generally $Q_{\mathrm{con}} = 0.2$ g/kg has been chosen for the in-cloud cloud water mass fraction Q_{con} (liquid and frozen) except for very large values of Q_{sat} (with $Q_{\mathrm{sat}} > 20$ g/kg) for which $Q_{\mathrm{con}} = 0.01\, Q_{\mathrm{sat}}$ is assumed. As above for Q_{sgs}, the partitioning of Q_{con} into liquid and ice clouds ($Q_{\mathrm{con}}^{\mathrm{water}}$ and $Q_{\mathrm{con}}^{\mathrm{ice}}$) is also determined by the coefficient f_{ice}.

Relating the in-cloud variables $Q_{\mathrm{sgs}}^{\mathrm{water}}$, Q_{sgs}^{ice}, $Q_{\mathrm{con}}^{\mathrm{water}}$ and $Q_{\mathrm{con}}^{\mathrm{ice}}$ to the effective, radiatively active variables $Q_{\mathrm{rad}}^{\mathrm{water}}$ and $Q_{\mathrm{rad}}^{\mathrm{ice}}$ requires a partitioning of the total cloud fraction $\mathcal{N} = CLC/100$ into a shallow convective part $\mathcal{N}_{\mathrm{con}}$ and the remaining subgrid part $(\mathcal{N} - \mathcal{N}_{\mathrm{con}})$. Following the COSMO model's subgrid scheme, $\mathcal{N}_{\mathrm{con}}$ is diagnosed from the total height $\left(H_{\mathrm{SC}}^{\mathrm{top}} - H_{\mathrm{SC}}^{\mathrm{bas}}\right)$ of shallow convective clouds as given in Eq. (A7) of the appendix. Using $\mathcal{N}_{\mathrm{con}}$ one can write

$$\begin{aligned} Q_{\mathrm{rad}}^{\mathrm{water}} &= Q_{\mathrm{con}}^{\mathrm{water}}\, \mathcal{N}_{\mathrm{con}} + Q_{\mathrm{sgs}}^{\mathrm{water}}\, (\mathcal{N} - \mathcal{N}_{\mathrm{con}})\ , \\ Q_{\mathrm{rad}}^{\mathrm{ice}} &= Q_{\mathrm{con}}^{\mathrm{ice}}\, \mathcal{N}_{\mathrm{con}} + Q_{\mathrm{sgs}}^{\mathrm{ice}}\, (\mathcal{N} - \mathcal{N}_{\mathrm{con}})\ , \end{aligned} \tag{3}$$

from which the corresponding values of LWC and IWC (in units of g/m^3) are given by

$$\mathrm{LWC} = Q_{\mathrm{rad}}^{\mathrm{water}} \cdot \rho \,, \qquad \mathrm{IWC} = Q_{\mathrm{rad}}^{\mathrm{ice}} \cdot \rho \simeq Q_{\mathrm{rad}}^{\mathrm{ice}} \cdot \rho_{\mathrm{d}} \,, \tag{4}$$

where ρ is the density of humid air and ρ_{d} is the density of dry air (in units g/m^3). The densities are determined using the ideal gas equation of state (A1). In the last step on the right of Eq. (4) the fact that ρ can be approximated by ρ_{d} at sufficiently low temperatures was used (which holds for the temperature range where ice processes are active in this scheme).

b. *Microphysical Parameterizations*

Once the total LWC and IWC from both grid-scale as well as subgrid-scale quantities have been calculated, further assumptions concerning the associated cloud microphysics have to be made. In particular, the effective radii of the scattering particles of solar radiation need to be estimated.

Following the assumptions in Bugliaro et al. (2011), the effective radii of water droplets in clouds are parameterized depending on LWC in units of g/m^3, droplet density N in units of m^{-3} and water density $\rho \approx 10^6$ g/m^3 at 4°C. The parameterization for the effective radius reads

$$R_{\mathrm{eff}}^{\mathrm{water}} = \left(\frac{3}{4} \cdot \frac{\mathrm{LWC}}{\pi \, k \, N \, \rho} \right)^{1/3} \,, \tag{5}$$

where $k = R_{\mathrm{vol}}^3 / R_{\mathrm{eff}}^3$ is the ratio between volumetric radius of droplets and the effective radius. For all examples given, $N = 1.5 \cdot 10^8\,\mathrm{m}^{-3}$ is chosen according to Bugliaro et al. (2011) and the value of $k = 0.67$ is chosen sensibly for mainly continental clouds according to Martin et al. (1994). Lower and upper limits on the effective radii of water droplets are taken to be 1 μm respectively 25 μm.

For ice crystals, a parameterization of randomly oriented hexagonal columns described in Bugliaro et al. (2011) is used who adopted from Wyser (1998) and McFarquhar et al. (2003). Similar as for water droplets, the effective radii of ice crystals in cirrus clouds depend on IWC in units of g/m^3 and temperature T in units of K as given by

$$
\begin{aligned}
B &= -2 + 10^{-3}\,(273\,\mathrm{K} - T)^{3/2} \cdot \log\left(\frac{\mathrm{IWC}}{50\,\mathrm{g/m^3}}\right) , \\
R_0 &\approx 377.4 + 203.3\,B + 37.91\,B^2 + 2.3696\,B^3 , \\
R_{\mathrm{eff}}^{\mathrm{ice}} &= \left(\frac{4}{4+\sqrt{3}}\right) \cdot R_0 .
\end{aligned}
\tag{6}
$$

Effective radii of the scattering ice particles calculated by Eqs. (6) are determined in μm. They are restricted to values between 20 μm and 90 μm.

4. Parallax Correction

In this section, a grid transformation on the input variables LWC, IWC, $R_{\mathrm{eff}}^{\mathrm{water}}$ and $R_{\mathrm{eff}}^{\mathrm{ice}}$ used by the RT solver is described which corrects the error due to the slant satellite viewing angle through the atmosphere. The correction is referred to as parallax correction.

Each grid box, defined by the indices (i, j, k) representing longitude, latitude, and altitude, respectively, is shifted horizontally by $(\Delta i, \Delta j)$ pixels. The Δi, Δj need to be chosen such that they correct the parallax. For this purpose, the shift should be

$$\Delta y = z_{\mathrm{top}} \tan\theta \, \sin\phi , \tag{7}$$

for the latitudinal direction, where ϕ is satellite azimuth angle, θ is the satellite zenith angle and z_{top} is the altitude of the upper boundary of the grid box, see Fig. 1. For the longitudinal direction, the shift should be

$$\Delta x = z_{\mathrm{top}} \tan\theta \, \cos\phi . \tag{8}$$

We discretize the shift by setting $(\Delta i, \Delta j)$ to rounded integers of $(\Delta x, \Delta y)$ divided by the grid resolution of 2.8 km.

The transformation mapping the input variables from the old to the new grid is thus carried out according to

$$\tilde{X}\left[i + \Delta i,\, j + \Delta j,\, k\right] = X\left[i, j, k\right] , \tag{9}$$

run over all grid boxes (i, j, k) where X refers to the three-dimensional arrays containing the variables LWC, IWC, $R_{\text{eff}}^{\text{water}}$ and $R_{\text{eff}}^{\text{ice}}$ and $\tilde{X}$ to their values on the new grid. Using the transformed grid to simulate RT in "independent column approximation" (ICA) takes the effect of the satellite viewing angles into account, however, with the advantage of using the faster 1D RT solver instead of the computationally expensive 3D RT solver. In section 5, the results including the parallax correction are compared to the uncorrected 1D operator results.

5. Accuracy Assessment

a. Experimental Setup

As mentioned above, 22 June 2011 has been chosen for the case study to assess the 1D operator accuracy. 3h-forecast fields of COSMO-DE are used to simulate synthetic satellite images in 3D and 1D at 06, 09, 12, 15 and 18 UTC. For this case study, observations are simulated for the Spinning Enhanced Visible and InfraRed Imager (SEVIRI) aboard the Meteosat 8 satellite of Meteosat Second Generation (MSG). Nonetheless, the forward operator introduced here is not limited to this particular instrument.

The satellite viewing angles on each individual pixel of the COSMO-DE domain are accounted for. In order to have a direct comparison between 3D and 1D RT, additional simplifications are made to ensure that no error is introduced due to different treatments in the calculations. The simplifications made are that the model levels, as well as the solar angles are kept constant over the scene at a particular time. Therefore, a constant SZA is assumed throughout the whole domain (corresponding to the pixel in the middle of the scene with latitude $50.8\,^{\circ}$ and longitude $10.4\,^{\circ}$). Given that we are only interested in the accuracy of the 1D operator as compared to a "perfect" 3D simulation, this slightly unrealistic model representation is acceptable.

To avoid errors due to boundary effects, a smaller grid of 390×420 pixels is used for the evaluation of the accuracy. The first reason for this is that the MYSTIC simulations use periodic boundary conditions which would introduce an error in our model truth at the boundaries. Secondly, COSMO-DE forecasts are integrated with boundary conditions obtained from the lower resolution COSMO-EU configuration. These introduce a kind of "driving" error at the edges of the model domain due to possible inconsistencies between COSMO-EU and COSMO-DE fields which also requires that the edges are neglected in future assimilation experiments. Removing 26 pixels in the north, 15 in the south, 15 in the west and 16 in the east of the original COSMO-DE domain, one can ensure that at least 42 km are cut off of each boundary.

The 3D MYSTIC simulations have been carried out with $N = 3 \cdot 10^4$ photons per pixel. In the cases at hand, the MYSTIC simulations have an uncertainty of about 1.3 % as calculated from Eq. (A.1) in Buras and Mayer (2011).

In order to quantify the relative difference between 3D and 1D simulations, we use the following formula

$$\frac{|\Delta R|}{R} = \frac{\sum_{i,j} \left| R_{ij}^{\mathrm{3D}} - R_{ij}^{\mathrm{1D}} \right|}{\sum_{i,j} R_{ij}^{\mathrm{3D}}}\,, \tag{10}$$

where the sums are calculated over all pixels of the relevant domain and R_{ij} is the reflectance in pixel (i, j). Unless stated otherwise, the term relative difference refers to the quantity defined in Eq. (10). Similarly, the relative bias is given by

$$\frac{\Delta R}{R} = \frac{\sum_{i,j} \left(R_{ij}^{\mathrm{3D}} - R_{ij}^{\mathrm{1D}} \right)}{\sum_{i,j} R_{ij}^{\mathrm{3D}}}\,. \tag{11}$$

b. Results

By looking at different times of the day, the dependence of the relative difference on the SZA is determined (Table 1). An example of the 3D and 1D operator output of a full COSMO-DE scene is depicted in Fig. 2. Comparing the two simulations, one can easily distinguish the main differences. Cloud shadows become apparent in the 3D simulation in this afternoon scene at 15 UTC with a SZA of 50°. These can not be captured by the 1D operator that simulates more homogeneous cloud structures.

Table 1 shows the results of the relative difference defined in Eq. (10) obtained using different corrections simulated for the VIS008 channel of MSG-SEVIRI varied over the SZA. For completeness, the corresponding solar azimuth angle (SAA) at each time is also given in the table (0° corresponds to the southern direction and the angle increases clockwise). "ICA" stands for the plain independent column approximation on 2.8 km resolution, "Parallax" denotes the 1D solver applied to the parallax corrected fields on 2.8 km resolution, "3×3-Mean" is a floating average of the parallax corrected version where the reflectance in each pixel is calculated by taking the floating average over 3×3 pixels (centered in the respective pixel). "5×5-Mean" denotes a floating average over 5×5 pixels.

Overall, the parallax correction improves the plain ICA result by about 2 %. Taking the floating average over 3×3 pixels smoothens the field and therefore eliminates errors due to small horizontal displacements which results in a further improvement by 1-2 %. Going to a smoothing over 5×5 pixels results in yet another small improvement. Between 06-15 UTC, the relative difference is smaller than 9 % in all cases while at 18 UTC, it increases significantly to over 20 % in the non-averaged cases. This strong increase in the differences is a result of the large SZA of 78° which leads to larger cloud shadows than in the earlier scenes. A sensitivity study, in which we artificially changed the SZA for the 18 UTC case to 50° (the value at 15 UTC), revealed that the difference is not very sensitive to the type of clouds involved. We conclude that for the assimilation of cloudy VIS and NIR reflectances, one might want to discard observations with a SZA larger than 70° or adjust the errors in the assimilation system unless further corrections are applied. The absolute value of the relative bias is very small (less than 0.6 %) for all simulated cases (Table 2).

To provide an example of the corresponding results for the SEVIRI channels VIS006 in the visible with a central wavelength of 635 nm and NIR016 in the near-infrared with the central wavelength at 1640 nm, 3D and parallax corrected 1D simulations have been carried out at 15 UTC. Fig. 3 shows the corresponding 3D operator output reflectance fields. For channel VIS006, the relative difference is 6.1 % with a bias of -0.4 % and for channel NIR016 it is 7.0 % with a bias of -1.2 %. We conclude that the accuracies are of similar magnitude for the two VIS channels while the NIR channel is slightly less accurate. The model cloud-cover at 15 UTC is depicted in Fig. 4. When comparing it to the RT simulations in Figs. 2 and 3 , it can be seen that the VIS channels mostly represent the lower and medium height (400-800 hPa) water clouds. The NIR channel is a good discriminator between ice clouds ($<$ 400 hPa) which appear dark due to the fact that ice absorbs stronger than liquid water at 1.6 μm and the water clouds which appear bright. In particular, the big thunderstorm cells can well be detected in the NIR. This may be a desirable feature since it provides information on the localization of deep convective clouds.

Fig. 5 depicts the relative differences $\left(R_{ij}^{\mathrm{3D}} - R_{ij}^{\mathrm{1D}}\right)/\frac{1}{2}\left(R_{ij}^{\mathrm{3D}} + R_{ij}^{\mathrm{1D}}\right)$ in reflectance between 3D and 1D calculation of channel VIS008 at 12 UTC in each pixel (i, j) of the evaluated domain as an example of the effect of the parallax correction. Without the correction, large differences are present near the edges of cloud structures. These differences are substantially reduced by applying the parallax correction in the 1D calculation. As a comparison, Fig. 5 also contains the 3D and parallax corrected 1D reflectance fields. It seems that the most severe relative differences occur at higher latitudes, in particular at sharp northern cloud edges where ice clouds are involved. A reasonable explanation for this is the fact that the southern position of the sun at noon produces the largest shadows north of the high clouds.

In addition, we separately analyzed areas where the differences are largest, i.e. at cloud edges. For this investigation, we have applied a threshold considering only those pixels in which the difference between 3D and 1D reflectance $|\Delta R| > 0.1$. For these pixels with a large difference, the effect of the parallax correction is even larger and the mean relative difference between 3D and ICA reduces from 31 % to 23 % with the parallax correction at 12 UTC.

To demonstrate how the synthetic scenes from model output look compared to the real observations from MSG-SEVIRI, we provide a time sequence of observations and simulations on 22 June 2011 in Fig. 6. The SEVIRI observations of channels VIS008 over the diurnal cycle are depicted in the top row, the middle row displays the 3D simulations from 3h-forecast fields and the bottom row shows the parallax corrected 1D simulations from 3h-forecast fields. On this particular day, the model forecasts contain substantially more clouds than the observations. These differences are mainly due to the discrepancy between COSMO-DE forecasts and reality. The forward operator developed here can therefore also be used as a tool to identify potential model weaknesses. To evaluate this in more detail, however, requires to compare a larger set of observed and simulated data which will be assessed in future studies.

Furthermore, Fig. 6 illustrates how the differences between synthetic 3D and 1D images depend on the SZA of the appropriate scene. At smaller angles around 09 or 12 UTC, it is hard to tell the difference between the two. With increasing angles at, e.g., 06 and 15 UTC, shadow effects become more obvious in the output of the 3D operator. For an even larger SZA at 18 UTC, they have a strong contribution to the 3D reflectances. This visually confirms the quantitative results from Table 1 described above.

6. Summary and Outlook

This article introduces an observation operator for VIS and NIR satellite reflectances. The operator is intended as a fast enough tool to study the impact of directly assimilating cloudy VIS and NIR observations within LETKF DA systems such as the pre-operational KENDA-COSMO system of DWD (or other DA systems that do not require a linearized and adjoint operator). Since particularly water clouds have a clearer signal at these wavelengths, it seems to be a natural extension to include such observations as a valuable source of cloud information. In addition to introducing the technical aspects of the forward operator, we have evaluated its accuracy with respect to a computationally very expensive Monte Carlo radiative transfer model.

Moreover, a parallax correction is introduced, which corrects 1D simulations for the slant path of radiation through the atmosphere towards the observing satellite. The accuracies of the independent-column calculation and its parallax corrected version are evaluated by comparison to 3D Monte Carlo simulations. The latter are considered as "perfect" model simulations due to their ability to account for arbitrarily complex cloud structures and corresponding shadow effects. Furthermore, the effect of horizontal averaging of the 3D and 1D reflectance fields over both 3×3 pixels and 5×5 pixels is evaluated to investigate the sensitivity of operator accuracy to resolution. The input fields are 3h-forecasts of the limited area COSMO model at 06, 09, 12, 15 and 18 UTC on 22 June 2011.

In summary, all relative differences between 06-15 UTC are about 6-8 % without parallax correction for the visible channel VIS008 of MSG-SEVIRI with a central wavelength of 810 nm. Including the parallax correction in the 1D calculations improves these results to about 4-6 %. The horizontal averaging over 3×3 and 5×5 pixels gives a further improvement to a difference of less than about 5 % and less than about 4.5 % respectively. This is due to the fact that the averaging cancels out some of the horizontal variations on small scales. Since the effective model resolution is lower than the grid size, similar smoothing routines might be relevant for future assimilation experiments to reduce the operator and observation error. In addition, given the deficiency of current models to capture every individual convective system, assimilating such observations at a reduced resolution may be a desirable approach. As examples, the differences in the two VIS and NIR channels of the SEVIRI instrument, VIS006 and NIR016, have also been evaluated at 15 UTC of the same day. The results for VIS006 are in the same ballpark as for VIS008 while NIR016 is about 1 % less accurate.

At 18 UTC, the differences turn out to be substantially larger than between 06-15 UTC due to the larger SZA leading to an increase in cloud shadows. In the absence of further corrections that can account for these 3D effects in the faster 1D simulations, one can draw the conclusion that for the assimilation of VIS and NIR satellite reflectance, it is only sensible to assimilate when solar zenith angles are smaller than about 70°. Due to the increased errors, observations at larger solar zenith angles however, can either be discarded or assimilated with a suitable adaption of the errors in the assimilation system.

In future studies, the 1D forward operator presented here shall be applied in the KENDA-COSMO system of DWD to study the impact of directly assimilating reflectance observations of MSG-SEVIRI solar channels. The presented 1D operator is reasonably fast for such case study purposes in an offline calculation. Nevertheless, a computation time of approximately 5-10 minutes per scene over the whole model domain (run on 37 processors) is beyond the limitations of an operational ensemble DA system. Thus, a second objective for future research is to test methods to accelerate RT in the VIS and NIR spectral range and assess the respective loss in accuracy. In addition to assimilation experiments, the observation operator can also be used for sensitivity studies as a tool to identify model weaknesses, in particular, concerning the representation of clouds.

Acknowledgments.

This study was carried out in the Hans–Ertel–Centre for Weather Research. This research network of Universities, Research Institutes and Deutscher Wetterdienst is funded by the BMVBS (Federal Ministry of Transport, Building and Urban Development). P.M.K. would like to thank Annika Schomburg, Christian Keil and Axel Seifert for discussions and help concerning COSMO related issues. P.M.K. is indebted to Luca Bugliaro for providing relevant satellite data.

APPENDIX

Relevant Formulae

In this appendix, relevant formulae and physical constants used in the operator calculations are shortly summarized. Note that the definitions used in the parameterizations of subgrid-scale quantities are adopted entirely from the subgrid scheme of the COSMO model code and are stated here for completeness only.

With pressure P and temperature T given, the densities are determined through the equation of state for ideal gases

$$\rho\, R\, T = P\,. \tag{A1}$$

For the gas constant of dry air, one can plug in the value $R_{\mathrm{d}} = 287.05\,\mathrm{m}^3\,\mathrm{Pa}\,\mathrm{kg}^{-1}\,\mathrm{K}^{-1}$ and for water vapor, it is given by $R_{\mathrm{v}} = 461.51\,\mathrm{m}^3\,\mathrm{Pa}\,\mathrm{kg}^{-1}\,\mathrm{K}^{-1}$.

The saturation vapor pressure over water and ice respectively is given by the Magnus formula

$$\begin{aligned} E^{\mathrm{water}} &\approx 610.78\,\mathrm{Pa}\cdot\exp\left(\frac{17.27\,(T-273.16\,\mathrm{K})}{T-35.86\,\mathrm{K}}\right)\,,\\ E^{\mathrm{ice}} &\approx 610.78\,\mathrm{Pa}\cdot\exp\left(\frac{21.87\,(T-273.16\,\mathrm{K})}{T-7.66\,\mathrm{K}}\right)\,. \end{aligned} \tag{A2}$$

Furthermore, the saturation mass fractions can be calculated as

$$Q^{\mathrm{x}}_{\mathrm{sat}} \approx \frac{\frac{R_{\mathrm{d}}}{R_{\mathrm{v}}}\,E^{\mathrm{x}}}{P-\left(1-\frac{R_{\mathrm{d}}}{R_{\mathrm{v}}}\right)E^{\mathrm{x}}}\,, \tag{A3}$$

from which one can derive the relative humidity $\varphi = Q_{\mathrm{tot}}/Q_{\mathrm{sat}}$ using the total humidity mass fraction $Q_{\mathrm{tot}} = Q_{\mathrm{V}} + Q_{\mathrm{C}} + Q_{\mathrm{I}}$. For x one can plug in either water or ice.

In the case of a mixed state the gas constant is, strictly speaking, not a constant but rather depends on pressure and temperature. It is given by

$$R = R_{\mathrm{d}}\cdot\left[1-\varphi\,\frac{E}{P}\left(1-\frac{R_{\mathrm{d}}}{R_{\mathrm{v}}}\right)\right]^{-1}\,, \tag{A4}$$

and takes on values between R_d and R_v.

In the following, some definitions are introduced which are used in the parameterizations summarized in section 3. The total saturation mass fraction is defined as a sum of water and ice contributions by

$$Q_\mathrm{sat} = Q_\mathrm{sat}^\mathrm{water}\,(1 - f_\mathrm{ice}) + Q_\mathrm{sat}^\mathrm{ice}\,f_\mathrm{ice}\,, \tag{A5}$$

where the ice fraction is defined as

$$f_\mathrm{ice} = 1 - \min\left(1, \max\left(0, \frac{(T - 273.15\,\mathrm{K}) + 25\,\mathrm{K}}{20\,\mathrm{K}}\right)\right)\,. \tag{A6}$$

In addition to the mass fractions, the COSMO model uses cloud fractions. The shallow convective cloud fraction in the subgrid scheme of the model is defined by

$$\mathcal{N}_\mathrm{con} = \min\left(1, \max\left(0.05, 0.35\,\frac{H_\mathrm{SC}^\mathrm{top} - H_\mathrm{SC}^\mathrm{bas}}{5000\,\mathrm{m}}\right)\right)\,, \tag{A7}$$

where the magnitude depends on the heights of the shallow convective clouds, $H_\mathrm{SC}^\mathrm{top}$ being the top height and $H_\mathrm{SC}^\mathrm{bas}$ the base height. The latter fields are model output in units of m. $H_\mathrm{SC}^\mathrm{top}$ and $H_\mathrm{SC}^\mathrm{bas}$ are non-zero where the convection scheme produces shallow convective clouds. If the height of the considered layer lies between $H_\mathrm{SC}^\mathrm{top}$ and $H_\mathrm{SC}^\mathrm{bas}$ Eq. (A7) is applied, otherwise we set $\mathcal{N}_\mathrm{con} = 0$.

REFERENCES

Baldauf, M., A. Seifert, J. Frstner, D. Majewski, and M. Raschendorfer, 2011: Operational convective-scale numerical weather prediction with the cosmo model: Description and sensitivities. *Monthly Weather Review*, **139**, 3887–3905.

Bauer, P., A. Geer, P. Lopez, and D. Salmond, 2010: Direct 4d-var assimilation of all-sky radiances. part i: Implementation. *Quarterly Journal of the Royal Meteorological Society*, **136**, 1868–1885.

Bauer, P., G. Ohring, C. Kummerow, and T. Auligne, 2011a: Assimilating satellite observations of clouds and precipitation into nwp models. *Bulletin of the American Meteorological Society*, **92**, ES25–ES28.

Bauer, P., et al., 2011b: Satellite cloud and precipitation assimilation at operational nwp centres. *Quarterly Journal of the Royal Meteorological Society*.

Baum, B., A. Heymsfield, P. Yang, and S. Bedka, 2005a: Bulk scattering models for the remote sensing of ice clouds. part i: Microphysical data and models. *J. Appl. Meteorol.*, **44**, 1885–1895.

Baum, B., P. Yang, A. Heymsfield, S. Platnick, M. King, Y.-X. Hu, and S. Bedka, 2005b: Bulk scattering models for the remote sensing of ice clouds. part ii: Narrowband models. *J. Appl. Meteorol.*, **44**, 1896–1911.

Baum, B., P. Yang, S. Nasiri, A. Heidinger, A. Heymsfield, and J. Li, 2007: Bulk scattering properties for the remote sensing of ice clouds: Part iii: High-resolution spectral models from 100 to 3250 cm^{-1}. *J. Appl. Meteorol. Climatol.*, **46**, 423–434.

Bennartz, R. and T. Greenwald, 2011: Current problems in scattering radiative transfer modelling for data assimilation. *Quarterly Journal of the Royal Meteorological Society.*

Bugliaro, L., T. Zinner, C. Keil, B. Mayer, R. Hollmann, M. Reuter, and W. Thomas, 2011: Validation of cloud property retrievals with simulated satellite radiances: a case study for seviri. *Atmos. Chem. Phys.*, **11**, 5603–5624.

Buras, R., T. Dowling, and C. Emde, 2011: New secondary-scattering correction in disort with increased efficiency for forward scattering. *Journal of Quantitative Spectroscopy and Radiative Transfer*, **112**, 2028–2034.

Buras, R. and B. Mayer, 2011: Efficient unbiased variance reduction techniques for monte carlo simulations of radiative transfer in cloudy atmospheres: the solution. *Journal of Quantitative Spectroscopy and Radiative Transfer*, **112**, 434–447.

Chandrasekhar, S., 1960: Radiative transfer. *Dover, Mineola, N.Y.*

Chevallier, F., P. Lopez, A. Tompkins, M. Janisková, and E. Moreau, 2004: The capability of 4d-var systems to assimilate cloud-affected satellite infrared radiances. *Quarterly Journal of the Royal Meteorological Society*, **130**, 917–932.

Emde, C. and B. Mayer, 2007: Simulation of solar radiation during a total eclipse: a challenge for radiative transfer. *Atmos. Chem. Phys.*, **7**, 2259–2270.

Errico, R., P. Bauer, and J. Mahfouf, 2007: Issues regarding the assimilation of cloud and precipitation data. *Journal of the Atmospheric Sciences*, **64**, 3785–3798.

Hunt, B., E. J. Kostelich, and I. Szunyogh, 2007: Efficient data assimilation for spatiotemporal chaos: A local ensemble transform kalman filter. *Physica D*, **230**, 112–126.

Kalnay, E., H. Li, T. Miyoshi, S. YANG, and J. BALLABRERA-POY, 2008: 4-d-var or ensemble kalman filter? *Tellus A*, **59**, 758–773.

Liou, K., 1992: Radiation and cloud processes in the atmosphere.

Marchuk, G. I., G. A. Mikhailov, and M. A. Nazaraliev, 1980: *The Monte Carlo methods in atmospheric optics*. Springer Series in Optical Sciences, Berlin: Springer, 1980.

Martin, G., D. Johnson, and A. Spice, 1994: The measurement and parameterization of effective radius of droplets in warm stratocumulus clouds. *J. Atmos. Sci.*, **51**, 1823–1842.

Matsumoto, M. and T. Nishimura, 1998: Mersenne twister. a 623-dimensionally equidistributed uniform pseudorandom number generator. *ACM Transactions on Modeling and Computer Simulation*, **8**, 3–30.

Mayer, B., 2009: Radiative transfer in the cloudy atmosphere. *European Physical Journal Conferences*, **1**, 75–99.

Mayer, B. and A. Kylling, 2005: Technical note: The libradtran software package for radiative transfer calculations: Description and examples of use. *Atmos. Chem. Phys.*, **5**, 1855–1877.

McFarquhar, G., S. Iacobellis, and R. Somerville, 2003: Scm simulations of tropical ice clouds using observationally based parameterizations of microphysics. *J. Climate*, **16**, 1643–1664.

McNally, A., 2002: A note on the occurrence of cloud in meteorologically sensitive areas and the implications for advanced infrared sounders. *Quarterly Journal of the Royal Meteorological Society*, **128**, 2551–2556.

McNally, A., 2009: The direct assimilation of cloud-affected satellite infrared radiances in the ecmwf 4d-var. *Quarterly Journal of the Royal Meteorological Society*, **135**, 1214–1229.

Pangaud, T., N. Fourrie, V. Guidard, M. Dahoui, and F. Rabier, 2009: Assimilation of airs radiances affected by mid-to low-level clouds. *Monthly Weather Review*, **137**, 4276–4292.

Pavelin, E., S. English, and J. Eyre, 2008: The assimilation of cloud-affected infrared satellite radiances for numerical weather prediction. *Quarterly Journal of the Royal Meteorological Society*, **134**, 737–749.

Pierluissi, J. and G. Peng, 1985: New molecular transmission band models for lowtran. *Opt. Eng.*, **24**, 541–547.

Renshaw, R. and P. Francis, 2011: Variational assimilation of cloud fraction in the operational met office unified model. *Quarterly Journal of the Royal Meteorological Society*, **137**, 1963–1974.

Richiazzi, P., S. Yang, C. Gautier, and D. Sowle, 1998: Sbdart: A research and teaching software tool for plane-parallel radiative transfer in the earth's atmosphere. *B. Am. Meteorol. Soc.*, **79**, 2101–2114.

Stamnes, K., S. Tsay, W. Wiscombe, and K. Jayaweera, 1988: Numerically stable algorithm for discrete-ordinate-method radiative transfer in multiple scattering and emitting layered media. *Appl. Opt.*, **27**, 2502–2509.

Stengel, M., M. Lindskog, P. Undén, and N. Gustafsson, 2012: The impact of cloud-affected ir radiances on forecast accuracy of a limited-area nwp model. *Quarterly Journal of the Royal Meteorological Society (in press).*

Stengel, M., M. Lindskog, P. Undén, N. Gustafsson, and R. Bennartz, 2010: An extended observation operator in hirlam 4d-var for the assimilation of cloud-affected satellite radiances. *Quarterly Journal of the Royal Meteorological Society*, **136**, 1064–1074.

Storto, A. and F. Tveter, 2009: Assimilating humidity pseudo-observations derived from the cloud profiling radar aboard cloudsat in aladin 3d-var. *Meteorological Applications*, **16**, 461–479.

Wiscombe, W., 1979, edited and revised 1996: Mie scattering calculations: Advances in technique and fast, vector-speed computer codes. *Tech. Report NCAR*, 416–444.

Wiscombe, W. and J. Evans, 1977: Exponential-sum fitting of radiative transmission functions. *J. Comput. Phys.*, **24**, 416–444.

Wyser, K., 1998: The effective radius in ice clouds. *J. Climate*, **11**, 1793–1802.

Zdunkowski, W., T. Trautmann, and A. Bott, 2007: Radiation in the atmosphere. *Cambridge University Press.*

List of Tables

Time	SZA	SAA	ICA	Parallax	3×3-Mean	5×5-Mean
06	66 °	262 °	7.6 %	6.0 %	5.3 %	4.7 %
09	38 °	302 °	6.1 %	4.1 %	3.2 %	2.7 %
12	28 °	19 °	6.1 %	3.9 %	2.8 %	2.2 %
15	50 °	78 °	8.3 %	5.9 %	4.8 %	4.0 %
18	78 °	112 °	23.1 %	21.2 %	19.1 %	17.3 %

TABLE 1. Relative difference from Eq. (10) between the results of the 3D simulations and the different 1D simulations depending on the SZA's for the SEVIRI channel VIS008 with a central wavelength of 810 nm.

Time	SZA	SAA	ICA	Parallax	3×3-Mean	5×5-Mean
06	66 °	262 °	0.39 %	0.47 %	0.47 %	0.47 %
09	38 °	302 °	-0.22 %	-0.42 %	-0.42 %	-0.42 %
12	28 °	19 °	0.24 %	-0.07 %	-0.07 %	-0.07 %
15	50 °	78 °	-0.22 %	-0.51 %	-0.51 %	-0.51 %
18	78 °	112 °	0.20 %	0.23 %	0.23 %	0.23 %

TABLE 2. Relative bias from Eq. (11) between the results of the 3D simulations and the different 1D simulations depending on the SZA's for the SEVIRI channel VIS008 with a central wavelength of 810 nm.

List of Figures

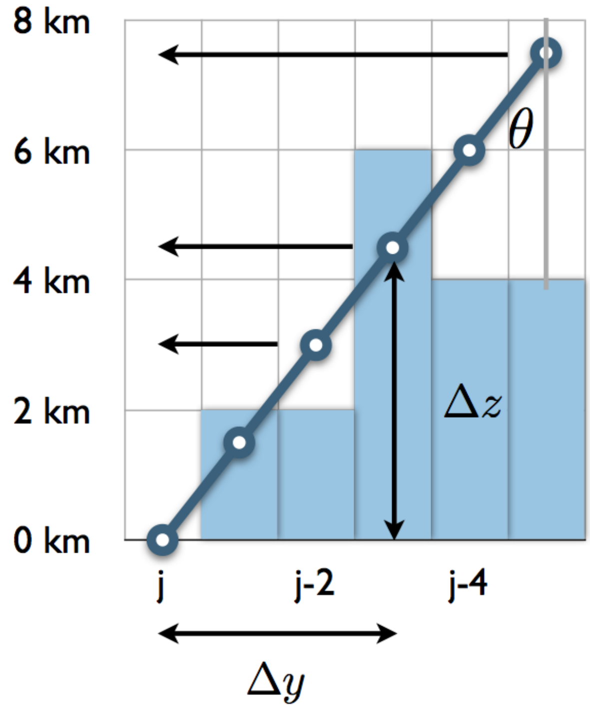

FIG. 1. Sketch of the pre-processing parallax correction routine applied to the input variables in a slice through the model atmosphere in south-north direction. The satellite zenith angle θ and distance Δz in km from the top height of a grid box z_{top} to the ground are used to calculate the shift Δy in km which is performed in the grid transformation.

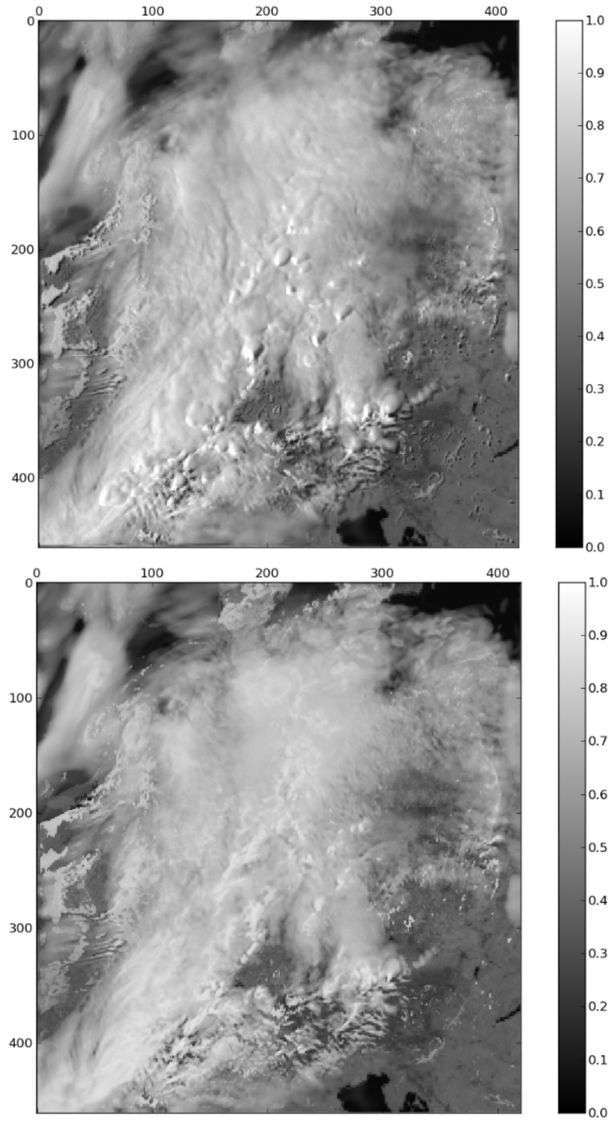

FIG. 2. Reflectance of a synthetic satellite image simulated with the 3D solver MYSTIC (upper plot) and with the parallax corrected 1D solver (lower plot) from COSMO-DE 3h-forecast fields at 15 UTC on June 22nd 2011 (SZA=50°). The central wavelength used is 810 nm which corresponds to the SEVIRI channel VIS008.

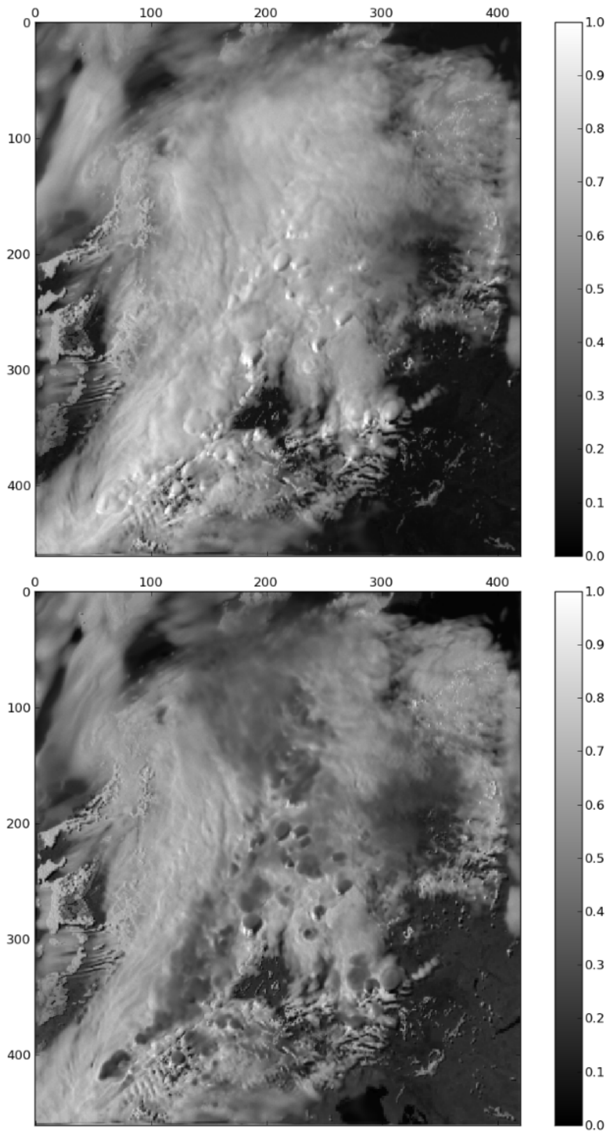

Fig. 3. Reflectance simulated with the 3D solver MYSTIC at 15 UTC on June 22nd 2011 (SZA=50°). The central wavelengths used are 635 nm corresponding to the SEVIRI channel VIS006 (upper plot) and 1640 nm corresponding to the SEVIRI channel NIR016 (lower plot).

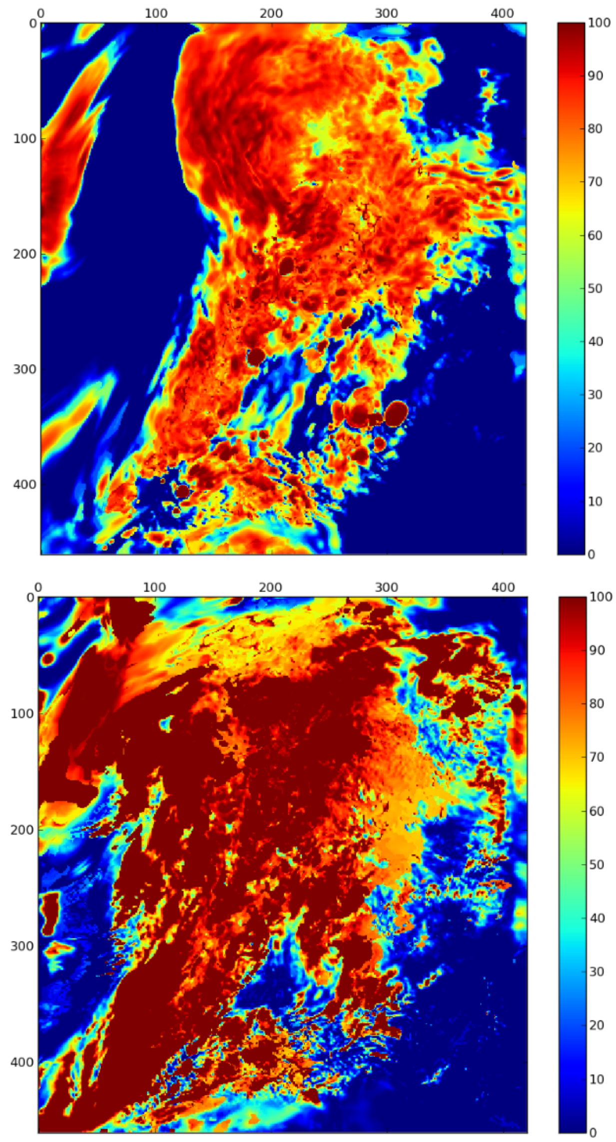

FIG. 4. COSMO-DE fields high cloud-cover (< 400 hPA) in the upper plot and medium cloud-cover (400-800 hPa) in the lower plot at 15 UTC in percent.

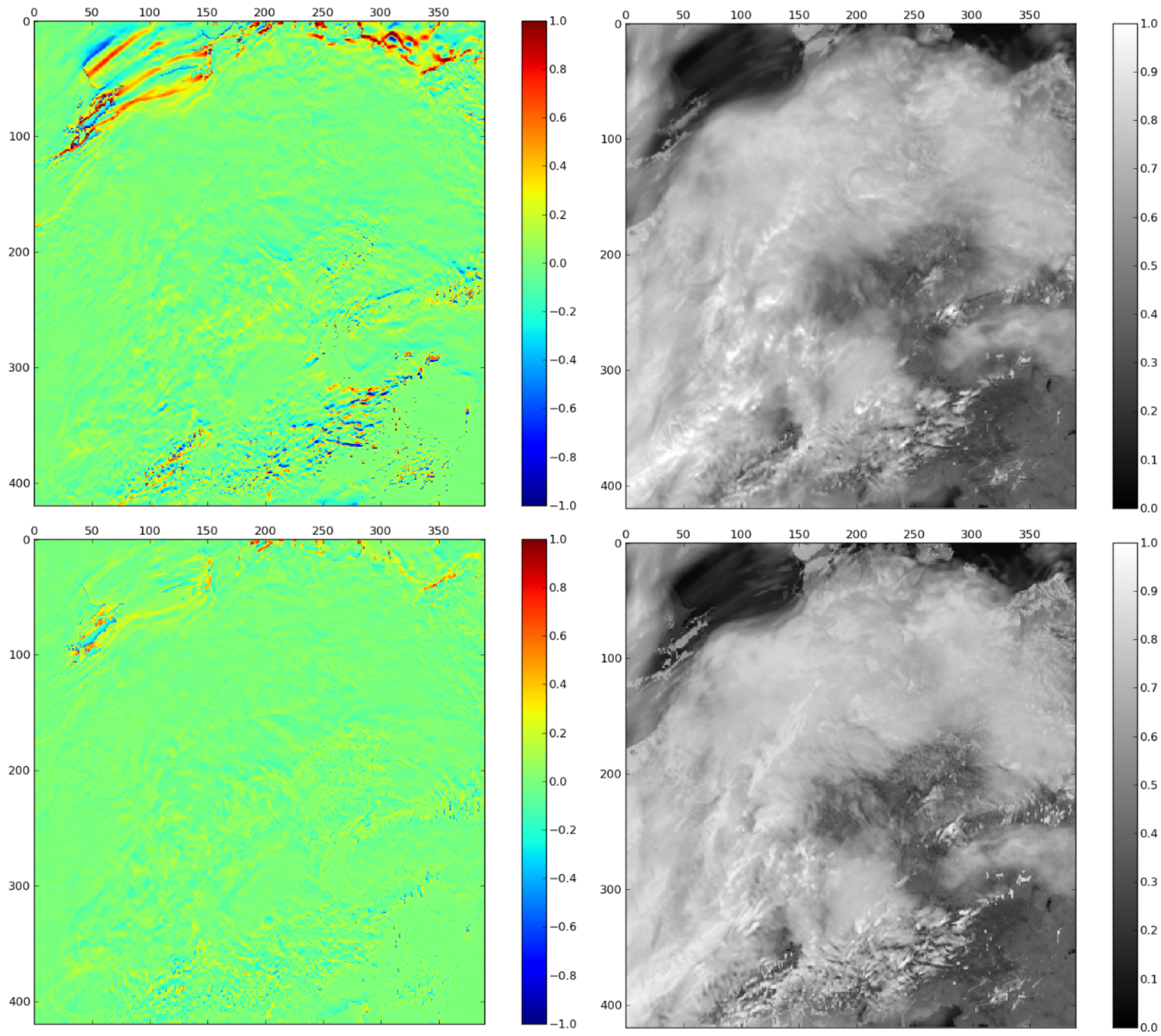

Fig. 5. Left: Relative difference in reflectance between 3D and 1D simulation at 12 UTC (SZA=28°) for the channel VIS008. The upper plot shows the result without any correction while in the lower plot, the parallax correction has been applied. Right: Corresponding 3D (upper plot) and parallax corrected 1D (lower plot) reflectance fields.

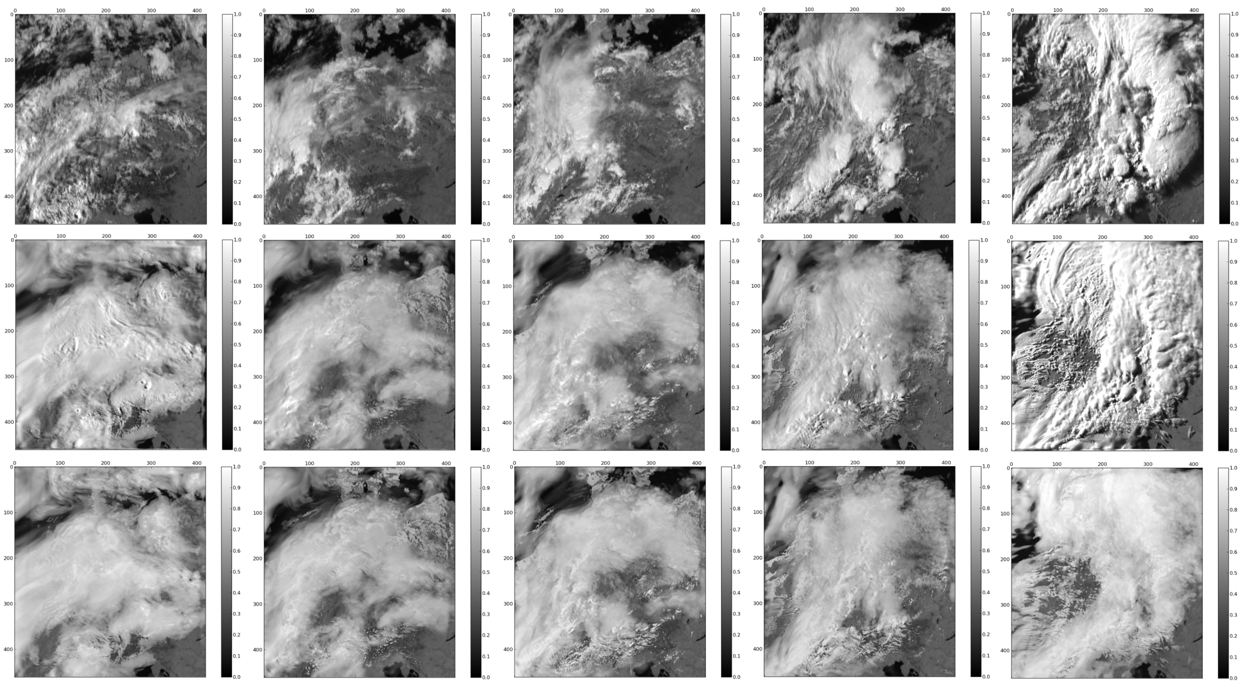

Fig. 6. Time sequence of SEVIRI observations (top row) versus 3D simulations (middle row) and 1D simulations (bottom row) every 3h from 06 to 18 UTC (left to right). The channel shown is VIS008.